

Chapter 4 Solar (and other) Neutrinos

4.1 Solar neutrino detectors

Careful analyses of the experiments that will be described below indicate that the observed solar neutrino fluxes differ substantially from standard solar model (SSM) expectations.

$$\phi(pp) \sim 0.9 \phi^{\text{SSM}}(pp)$$

$$\phi(^7\text{Be}) \sim 0$$

$$\phi(^8\text{B}) \sim 0.43 \phi^{\text{SSM}}(^8\text{B})$$

This pattern is difficult to reproduce in a solar model because of the temperature dependences of the neutrino fluxes

$$\phi(pp) \propto T_c^{-1.2} \quad \phi(^7\text{Be}) \propto T_c^8 \quad \phi(^8\text{B}) \propto T_c^{18}$$

(These results come from our standard formula, *but* with the constraint imposed that the solar luminosity be correctly reproduced. This means that the ppI cycle production must go *up* as the temperature goes down in order to produce the desired luminosity.) A reduced ^8B neutrino flux can be produced by lowering the central temperature of the sun somewhat. However, such adjustments, either by varying the parameters of the SSM or by adopting some nonstandard physics, tend to push the $\phi(^7\text{Be})/\phi(^8\text{B})$ ratio to higher values rather than the low one above,

$$\frac{\phi(^7\text{Be})}{\phi(^8\text{B})} \sim T_c^{-10}$$

Thus the observations seem difficult to reconcile with plausible solar model variations.

As of 1998 five solar neutrino experiments had provided data, the Homestake ^{37}Cl experiment, the gallium experiments SAGE and GALLEX, Kamiokande, and SuperKamiokande. The first three detectors are radiochemical, while Kamiokande and SuperKamiokande record neutrino-electron elastic scattering event-by-event.

The Homestake Experiment

Detection of neutrinos by the reaction $^{37}\text{Cl}(\nu_e, e)^{37}\text{Ar}$ was suggested independently by Pontecorvo (1946) and by Alvarez (1949). Davis's efforts to mount a 0.61 kiloton experiment using perchloroethylene (C_2Cl_4) were greatly helped by Bahcall's demonstration that transitions to excited states in ^{37}Ar , particularly the Fermi transition to the analog state at 4.99 MeV, increased the ^8B cross section by a factor of 40. This suggested that Davis's detector would have the requisite sensitivity to detect ^8B neutrinos, thereby accurately determining the central temperature of the sun. The experiment was mounted in the Homestake Gold Mine, Lead, South Dakota, in a cavity constructed approximately 4850 feet underground [4280 meters water equivalent (m.w.e.)]. It operated almost continuously since 1967, finally

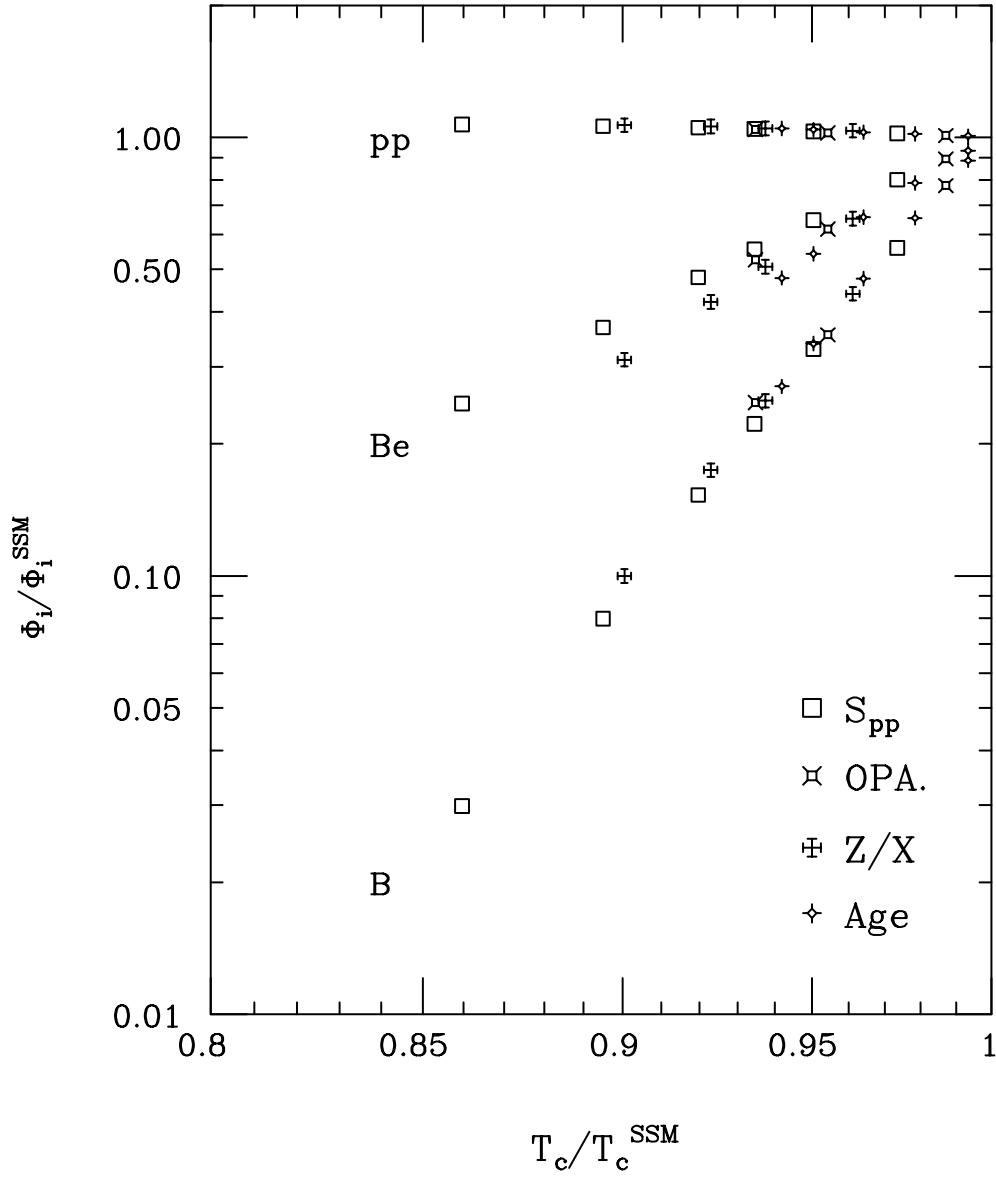


Figure 1: Here a variety of nonstandard solar models have been evaluated, where quantities like nuclear S-factors, the opacity, the solar age, and the metal content have varied outside their accepted uncertainties. The resulting neutrino fluxes and the core temperature are evaluated, and the former are plotted versus the latter. One sees that core temperature gives a very good one-parameter description of the results: this quantity seems to govern the neutrino fluxes, regardless of the source of the nonstandard model variation. One also sees that a reduced ^8B neutrino flux requires a cooler sun, while a reduced $^7\text{Be}/^8\text{B}$ neutrino flux ratio would require a hotter one. This graph is from Castellani et al.

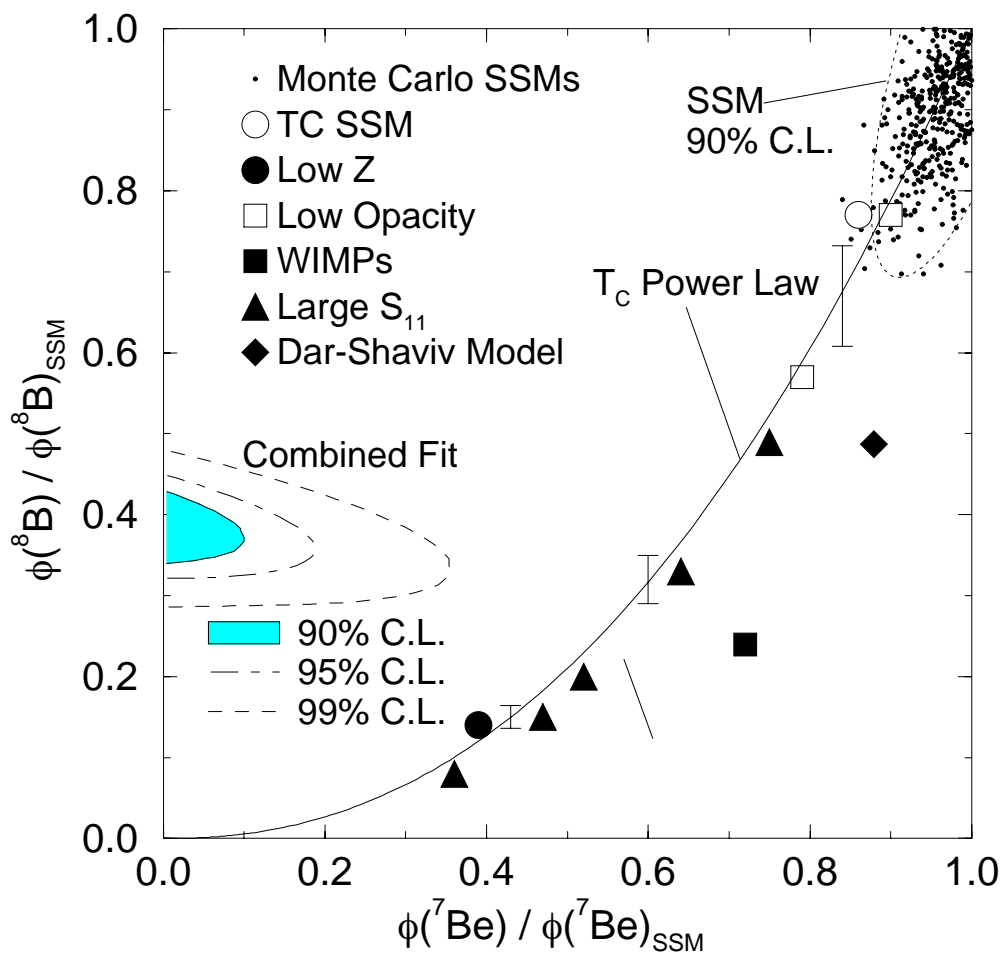


Figure 2: Nonstandard solar models are again evaluated, and when their relative ${}^7\text{Be}$ and ${}^8\text{B}$ fluxes are plotted, they form a path in the lower right quadrant. However the experimental data is in the upper left quadrant (and in fact prefers a ${}^7\text{Be}$ neutrino flux that is negative!) This shows that it is hard to fit the data assuming standard neutrino physics (especially an undistorted ${}^8\text{B}$ neutrino profile). From Hata et al.

terminating in 2002, when the Homestake Mine closed. The result of 25 years of measurement is

$$\langle\sigma\phi\rangle_{^{37}\text{Cl}} = 2.55 \pm 0.17 \pm 0.18 \text{ SNU} \quad (1\sigma)$$

which can be prepared to two recent standard solar model predictions of 8.0 ± 1.0 SNU and 6.4 ± 1.4 SNU, all with 1σ errors. The ^8B and ^7Be contributions account for about 75% and 16% of the total.

The experiment depends on the special properties of ^{37}Ar : as a noble gas, it can be removed readily from perchloroethylene, while its half life ($\tau_{1/2} = 35$ days) allows both a reasonable exposure time and counting of the gas as it decays back to ^{37}Cl . Argon is removed from the tank by a helium purge, and the gas then circulated through a condenser, a molecular sieve, and a charcoal trap cooled to the temperature of liquid nitrogen. Typically $\sim 95\%$ of the argon in the tank is captured in the trap. (The efficiency is determined each run from the recovery results for a known amount of carrier gas, ^{36}Ar or ^{38}Ar , introduced into the tank at the start of the run.) When the extraction is completed, the trap is heated and swept by He. The extracted gas is passed through a hot titanium filter to remove reactive gases, and then other noble gases are separated by gas chromatography. The purified argon is loaded into a small proportional counter along with tritium-free methane, which serves as a counting gas. Since the electron capture decay of ^{37}Ar leads to the ground state of ^{37}Cl , the only signal for the decay is the 2.82 keV Auger electron produced as the atomic electrons in ^{37}Cl adjust to fill the K-shell vacancy. The counting of the gas typically continues for about one year (~ 10 half lives).

The measured cosmic ray-induced background in the Homestake detector is 0.06 ^{37}Ar atoms/day while neutron-induced backgrounds are estimated to be below 0.03 atoms/day. A signal of 0.48 ± 0.04 atoms/day is attributed to solar neutrinos. When detector efficiencies, ^{37}Ar decays occurring in the tank, etc., are taken into account, the number of ^{37}Ar atoms counted is about 25/year.

The Kamiokande and SuperKamiokande Experiments

The Kamiokande experiment used a 4.5 kiloton cylindrical imaging water Cerenkov detector originally designed for proton decay searches, but later reinstrumented to detect low energy neutrinos. It detected neutrinos by the Cerenkov light produced by recoiling electrons in the reaction

$$\nu_x + e \rightarrow \nu'_x + e'$$

Both ν_e and heavy flavor neutrinos contribute, with $\sigma(\nu_e)/\sigma(\nu_\mu) \sim 7$. The light was detected by photomultiplier tubes that viewed the inner volume of the detector. Kamiokande had an inner fiducial volume of 0.68 kilotons. Its successor, SuperKamiokande, then ran fully instrumented for a number of years, collecting 1496 days of data. (SuperKamiokande had a phototube accident and is now running with about half of the original number of tubes.) SuperKamiokande has a much larger fiducial volume of 22.5 kilotons.

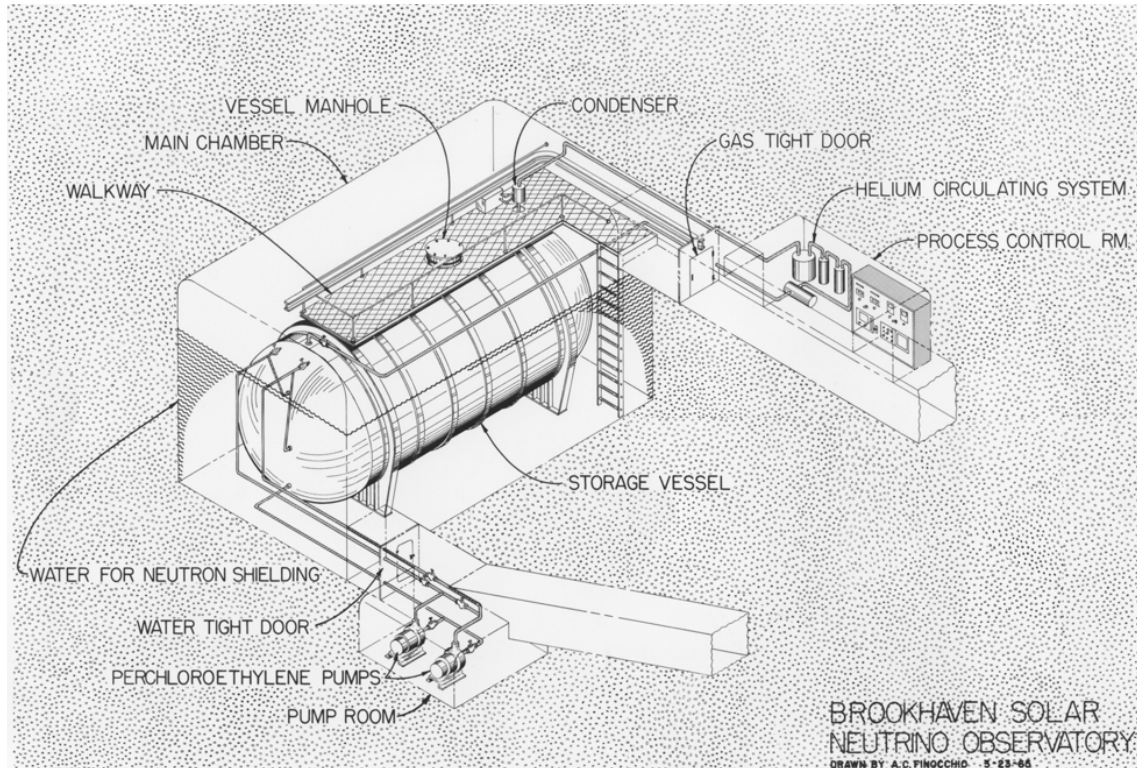


Figure 3: A schematic and a photo of the chlorine experiment. This detector operated from 1965 through 2002. From Brookhaven National Laboratory archives.

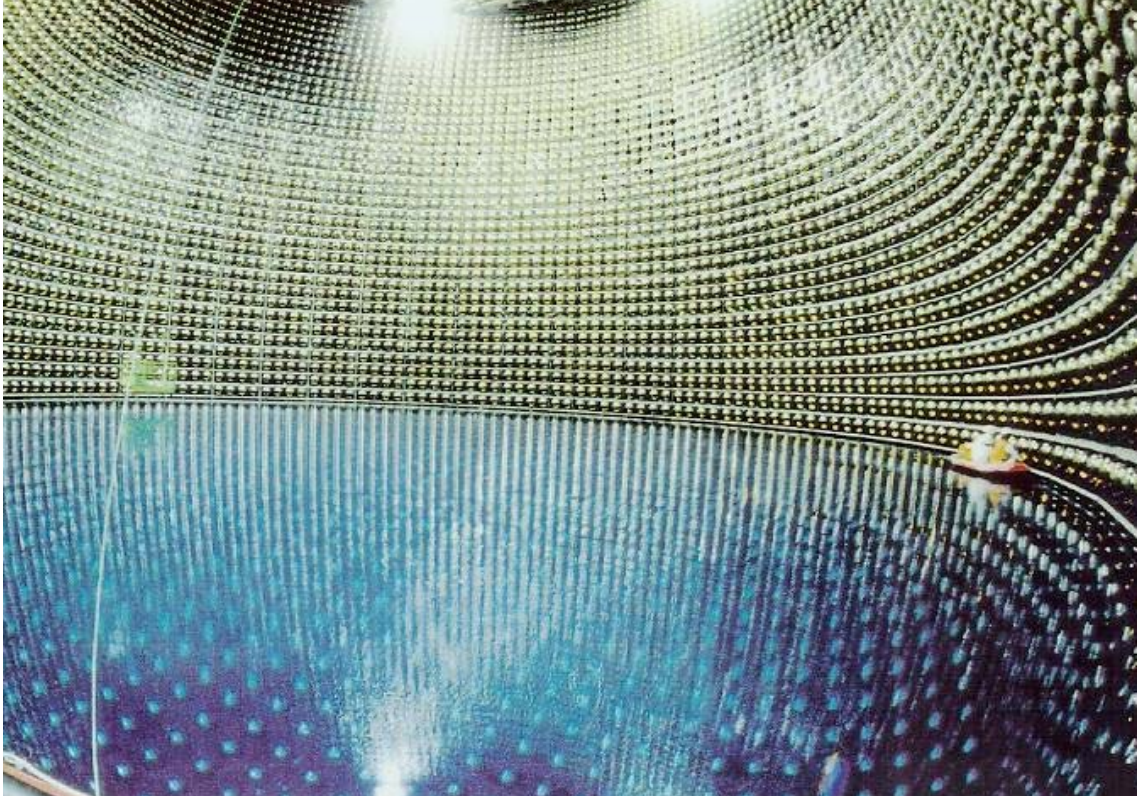


Figure 4: Super-Kamiokande at the point where the detector was first filled. The scientists are cleaning the phototube surfaces as the water rises. Photo by the Super-Kamiokande collaboration.

Kamiokande was (SuperKamiokande is) sensitive to the high energy portion of the ${}^8\text{B}$ neutrino spectrum. Between December, 1985, and July, 1993, Kamiokande accumulated 1667 live detector days of data. Under the assumption that the incident neutrinos are ν_e s with an undistorted ${}^8\text{B}$ β decay spectrum, the Kamiokande data gave

$$\phi_{\nu_e}({}^8\text{B}) = (2.91 \pm 0.08 \pm 0.12) \cdot 10^6 / \text{cm}^2 \text{ s} \quad (1\sigma)$$

The total number of detected solar neutrino events was 476_{-34}^{+36} .

The corresponding result from SuperKamiokande obtained in 1496 effective days of running is

$$\phi({}^8\text{B}) = 2.35 \pm 0.02 \pm 0.08 \times 10^6 / \text{cm}^2 \text{ sec}$$

This is about 46% of the standard solar model flux prediction. Note that SuperKamiokande has already substantially surpassed Kamiokande in accuracy.

These experiments are remarkable in several respects. They are the first detectors to measure solar neutrinos in real time. Essential to the method is the sharp peaking of the electron

angular distribution in the direction of the incident neutrino: this forward peaking allows the experimenters to separate solar neutrino events from an isotropic background. The unambiguous observation of a peak in the cross section correlated with the position of the sun is the first direct demonstration that the sun produces neutrinos as a byproduct of fusion.

The SAGE and GALLEX Experiments

Two radiochemical gallium experiments exploiting the reaction ${}^{71}\text{Ga}(\nu_e, e){}^{71}\text{Ge}$, SAGE and GALLEX, began solar neutrino measurements in January, 1990, and May, 1991, respectively. SAGE operated in the Baksan Neutrino Observatory, under 4700 m.w.e. of shielding from Mount Andyrchi in the Caucasus, while GALLEX was housed in the Gran Sasso Laboratory at a depth of 3300 m.w.e. These experiments are sensitive primarily to the low-energy pp neutrinos, the flux of which is sharply constrained by the solar luminosity in any steady-state model of the sun. The gallium experiment was first suggested by Kuzmin in 1966. In 1974 Ray Davis and collaborators began work to develop a practical experimental scheme. Their efforts, in which both GaCl_3 solutions and Ga metal targets were explored, culminated with the 1.3-ton Brookhaven/Heidelberg/Rehovot/Princeton pilot experiment in 1980-82 that demonstrated the procedures later used by GALLEX. SAGE used a liquid metal target.

SAGE began operations with 30 tons of gallium, and later increased to 55 tons. The result is

$$\langle\sigma\phi\rangle_{71\text{Ge}} = 75.4_{-6.8}^{+7.0} (\text{stat})_{-3.0}^{+3.5} (\text{sys}) \text{ SNU} \quad (1\sigma)$$

The corresponding result from GALLEX (and its successor GNO) is

$$\langle\sigma\phi\rangle_{71\text{Ge}} = 74.1 \pm 6.8 \text{ SNU} \quad (1\sigma)$$

These results are 59% and 58% of the SSM prediction. Both detectors were tested with neutrino sources, marking the first time such calibrations of solar neutrino detectors had been made.

The nuclear physics of the reaction ${}^{71}\text{Ga}(\nu_e, e){}^{71}\text{Ge}$ accounts for its sensitivity to low-energy neutrinos. As the threshold is 233 keV, the ground state (and first excited state) can be excited by pp neutrinos. The ground-state cross section can be determined from the measured electron capture lifetime of ${}^{71}\text{Ge}$, and is quite strong. The low-energy pp neutrinos account for about 55% of the capture rate. Because of this strong pp neutrino contribution, there exists a minimal astronomical counting rate of 79 SNU for the Ga detector that assumes only a steady-state sun and standard model weak interaction physics. This minimum value corresponds to a sun that produces the observed luminosity entirely through the ppI cycle. The rates found by SAGE and GALLEX are quite close to this bound.

4.2 Neutrino masses and vacuum neutrino oscillations

One odd feature of particle physics is that neutrinos, which are not required by any symmetry to be massless, nevertheless must be much lighter than any of the other known fermions. For instance, the current limit on the $\bar{\nu}_e$ mass is $\lesssim 5$ eV. The standard model requires neutrinos

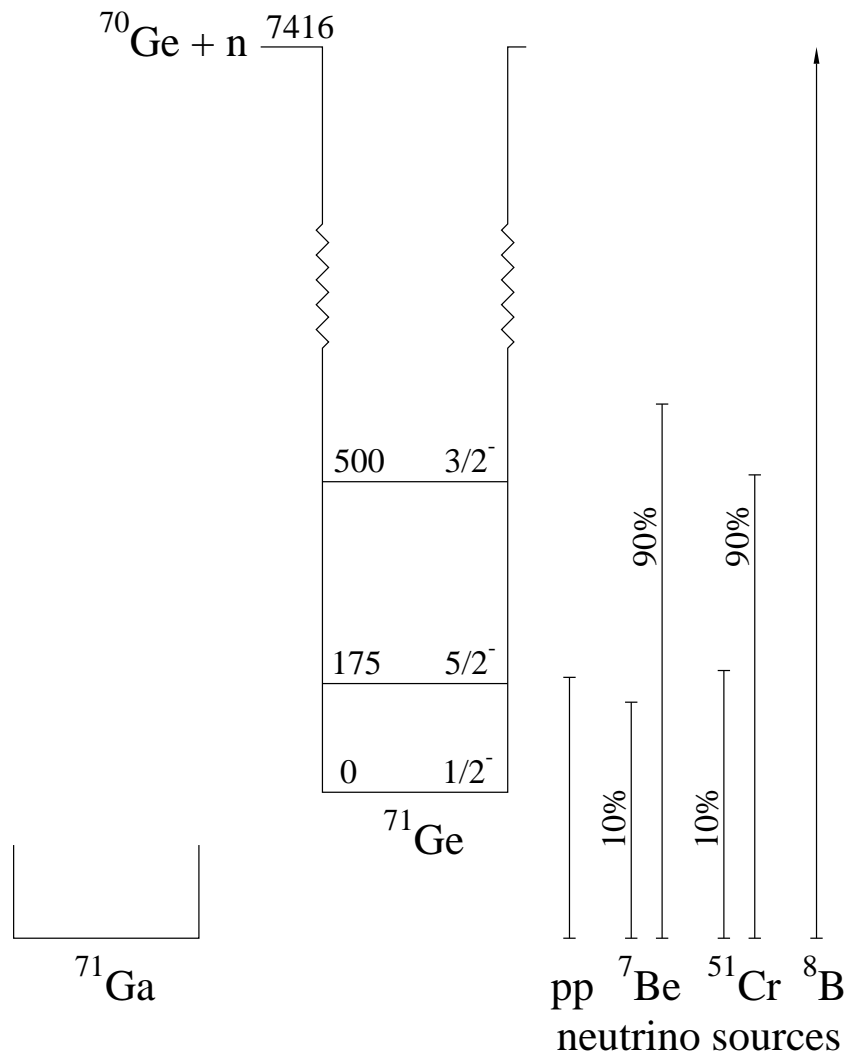


Figure 5: The level diagram for $^{71}\text{Ga}/^{71}\text{Ge}$ showing the excitations induced by pp and ^7Be neutrinos.

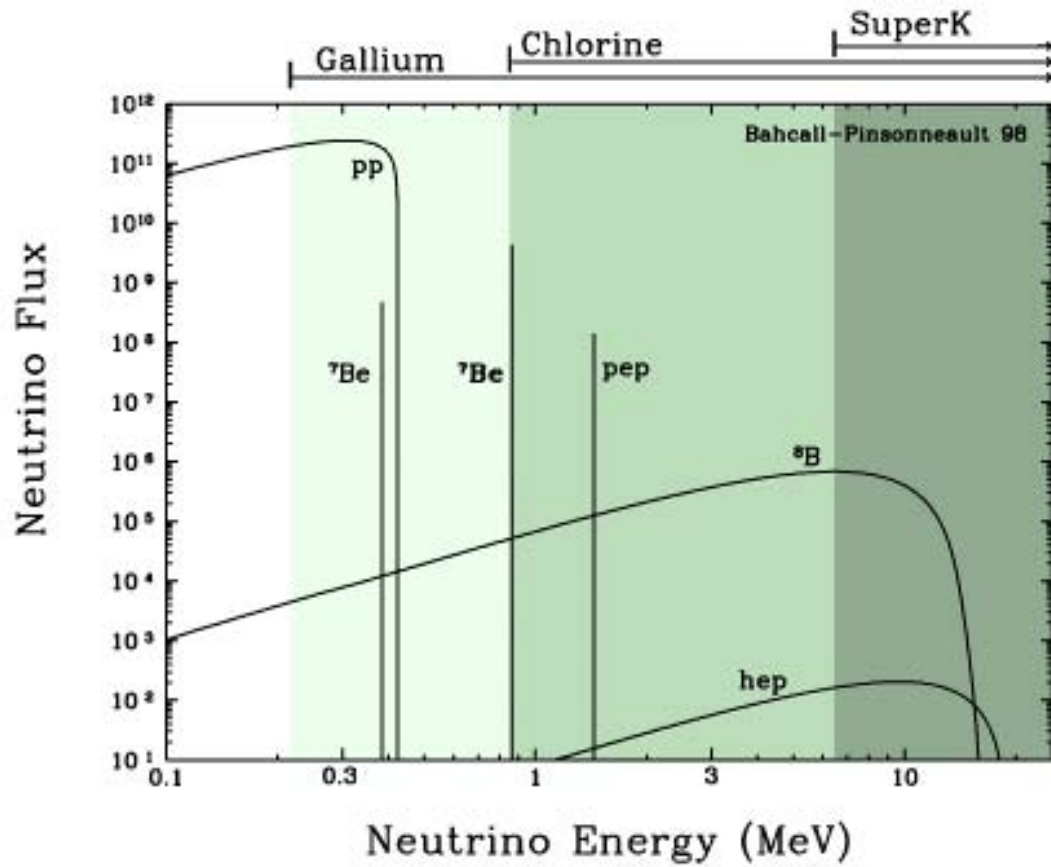


Figure 6: The sensitivities of various experiments to different portions of the solar neutrino spectrum are illustrated. From Bahcall.

to be massless, but the reasons are not fundamental. Dirac mass terms m_D , analogous to the mass terms for other fermions, cannot be constructed because the model contains no right-handed neutrino fields. Neutrinos can also have Majorana mass terms

$$\overline{\nu}_L^c m_L \nu_L \quad \text{and} \quad \overline{\nu}_R^c m_R \nu_R$$

where the subscripts L and R denote left- and right-handed projections of the neutrino field ν , and the superscript c denotes charge conjugation. The first term above is constructed from left-handed fields, but can only arise as a nonrenormalizable effective interaction when one is constrained to generate m_L with the doublet scalar field of the standard model. The second term is absent from the standard model because there are no right-handed neutrino fields.

None of these standard model arguments carries over to the more general, unified theories that theorists believe will supplant the standard model. In the enlarged multiplets of extended models it is natural to characterize the fermions of a single family, e.g., ν_e , e , u , d , by the same mass scale m_D . Small neutrino masses are then frequently explained as a result of the Majorana neutrino masses. In the seesaw mechanism,

$$M_\nu \sim \begin{pmatrix} 0 & m_D \\ m_D^T & m_R \end{pmatrix}$$

Diagonalization of the mass matrix produces one light neutrino, $m_{\text{light}} \sim \frac{m_D^2}{m_R}$, and one unobservably heavy, $m_{\text{heavy}} \sim m_R$. The factor (m_D/m_R) is the needed small parameter that accounts for the distinct scale of neutrino masses. The masses for the ν_e , ν_μ , and ν_τ are then related to the squares of the corresponding quark masses m_u , m_c , and m_t . Taking $m_R \sim 10^{16}$ GeV, a typical grand unification scale for models built on groups like SO(10), the seesaw mechanism gives the crude relation

$$m_{\nu_e} : m_{\nu_\mu} : m_{\nu_\tau} \leftrightarrow 2 \cdot 10^{-12} : 2 \cdot 10^{-7} : 3 \cdot 10^{-3} eV.$$

The fact that solar neutrino experiments can probe small neutrino masses, and thus provide insight into possible new mass scales m_R that are far beyond the reach of direct accelerator measurements, has been an important theme of the field.

Now one of the most interesting possibilities for solving the solar neutrino problem has to do with neutrino masses. For simplicity we will discuss just two neutrinos. If a neutrino has a mass m , we mean that as it propagates through free space, its energy and momentum are related in the usual way for this mass. Thus if we have two neutrinos, we can label those neutrinos according to the eigenstates of the free Hamiltonian, that is, as mass eigenstates.

But neutrinos are produced by the weak interaction. In this case, we have another set of eigenstates, the flavor eigenstates. We can define a ν_e as the neutrino that accompanies the positron in β decay. Likewise we label by ν_μ the neutrino produced in muon decay.

Now the question: are the eigenstates of the free Hamiltonian and of the weak interaction Hamiltonian identical? Most likely the answer is no: we know this is the case with the quarks, since the different families (the analog of the mass eigenstates) do interact through the weak interaction. That is, the up quark decays not only to the down quark, but also occasionally to the strange quark. (This is why we had a $\cos \theta_c$ in our β decay amplitude: the amplitude for $u \rightarrow s$ is proportional to $\sin \theta_c$.) Thus we suspect that the weak interaction and mass eigenstates, while spanning the same two-neutrino space, are not coincident: the mass eigenstates $|\nu_1\rangle$ and $|\nu_2\rangle$ (with masses m_1 and m_2) are related to the weak interaction eigenstates by

$$\begin{aligned} |\nu_e\rangle &= \cos \theta_v |\nu_1\rangle + \sin \theta_v |\nu_2\rangle \\ |\nu_\mu\rangle &= -\sin \theta_v |\nu_1\rangle + \cos \theta_v |\nu_2\rangle \end{aligned}$$

where θ_v is the (vacuum) mixing angle.

An immediate consequence is that a state produced as a $|\nu_e\rangle$ or a $|\nu_{mu}\rangle$ at some time t - for example, a neutrino produced in β decay - does not remain a pure flavor eigenstate as it propagates away from the source. This is because the different mass eigenstates comprising the neutrino will accumulate different phases as they propagate downstream, a phenomenon known as vacuum oscillations (vacuum because the experiment is done in free space). To see the effect, suppose we produce a neutrino in some β decay where we measure the momentum of the initial nucleus, final nucleus, and positron. Thus the outgoing neutrino is a momentum eigenstate. At time $t=0$, then

$$|\nu(t=0)\rangle = |\nu_e\rangle = \cos \theta_v |\nu_1\rangle + \sin \theta_v |\nu_2\rangle$$

Each eigenstate subsequently propagates with a phase

$$e^{i(\vec{k}\cdot\vec{x}-\omega t)} = e^{i(\vec{k}\cdot\vec{x}-\sqrt{m_i^2+k^2}t)}$$

But if the neutrino mass is small compared to the neutrino momentum/energy, one can write

$$\sqrt{m_i^2 + k^2} \sim k \left(1 + \frac{m_i^2}{2k^2}\right)$$

Thus we conclude

$$\begin{aligned} |\nu(t)\rangle &= e^{i(\vec{k}\cdot\vec{x}-kt - \frac{(m_1^2+m_2^2)}{4k}t)} \\ &\times [\cos \theta_v |\nu_1\rangle e^{i\delta m^2 t/4k} + \sin \theta_v |\nu_2\rangle e^{-i\delta m^2 t/4k}] \quad (eq.A) \end{aligned}$$

We see there is a common average phase (which has no physical consequence) as well as a beat phase that depends on

$$\delta m^2 = m_2^2 - m_1^2$$

Now it is a simple matter to calculate the probability that our neutrino state remains a $|\nu_e\rangle$ at time t

$$P_{\nu_e}(t) = |\langle \nu_e | \nu(t) \rangle|^2$$

$$= 1 - \sin^2 2\theta_v \sin^2 \left(\frac{\delta m^2 t}{4k} \right) \rightarrow 1 - \frac{1}{2} \sin^2 2\theta_v$$

where the limit on the right is appropriate for large t . Now $E \sim k$, where E is the neutrino energy, by our assumption that the neutrino masses are small compared to k . Thus we can reinsert the units above to write the probability in terms of the distance x of the neutrino from its source,

$$P_\nu(x) = 1 - \sin^2 2\theta_v \sin^2 \left(\frac{\delta m^2 c^4 x}{4\hbar c E} \right)$$

(When one properly describes the neutrino state as a wave packet, the large-distance behavior follows from the eventual separation of the mass eigenstates.) If the the oscillation length

$$L_o = \frac{4\pi\hbar c E}{\delta m^2 c^4}$$

is comparable to or shorter than one astronomical unit, a reduction in the solar ν_e flux would be expected in terrestrial neutrino oscillations.

The suggestion that the solar neutrino problem could be explained by neutrino oscillations was first made by Pontecorvo in 1958, who pointed out the analogy with $K_0 \leftrightarrow \bar{K}_0$ oscillations. From the point of view of particle physics, the sun is a marvelous neutrino source. The neutrinos travel a long distance and have low energies (~ 1 MeV), implying a sensitivity to

$$\delta m^2 \gtrsim 10^{-12} eV^2. \tag{1}$$

In the seesaw mechanism, $\delta m^2 \sim m_2^2$, so neutrino masses as low as $m_2 \sim 10^{-6} eV$ could be probed. In contrast, terrestrial oscillation experiments with accelerator or reactor neutrinos are typically limited to $\delta m^2 \gtrsim 0.1 eV^2$.

From the expressions above one expects vacuum oscillations to affect all neutrino species equally, if the oscillation length is small compared to an astronomical unit. This appears to contradict observation, as the pp flux may not be significantly reduced. Furthermore, the theoretical prejudice that θ_v should be small makes this an unlikely explanation of the significant discrepancies with SSM ${}^7\text{Be}$ and ${}^8\text{B}$ flux predictions.

The first objection, however, can be circumvented in the case of “just so” oscillations where the oscillation length is comparable to one astronomical unit. In this case the oscillation probability becomes sharply energy dependent, and one can choose δm^2 to preferentially suppress one component (e.g., the monochromatic ${}^7\text{Be}$ neutrinos). This scenario has been explored by several groups and remains an interesting possibility. However, the requirement of large mixing angles remains.

Below we will see that stars allow us to “get around” this problem with small mixing angles. In preparation for this, we first present the results above in a slightly more general way. The

analog of the result marked Eq.A above for an initial muon neutrino ($|\nu(t=0)\rangle = |\nu_\mu\rangle$) can be derived and is

$$|\nu(t)\rangle = e^{i(\vec{k}\cdot\vec{x}-kt-\frac{(m_1^2+m_2^2)}{4k}t)} \\ \times [-\sin\theta_\nu|\nu_1\rangle e^{i\delta m^2 t/4k} + \cos\theta_\nu|\nu_2\rangle e^{-i\delta m^2 t/4k}] \quad (\text{eq.B})$$

Now if we compare eqs. (A) and (B) we see that they are special cases of a more general problem. Suppose we write our initial neutrino wave function in the most general form

$$|\nu(t=0)\rangle = a_e(t=0)|\nu_e\rangle + a_\mu(t=0)|\nu_\mu\rangle$$

Then eqs. (A) and (B) tell us that the subsequent propagation is described by changes in $a_e(x)$ and $a_\mu(x)$ according to (this takes a bit of algebra)

$$i\frac{d}{dx} \begin{pmatrix} a_e \\ a_\mu \end{pmatrix} = \frac{1}{4E} \begin{pmatrix} -\delta m^2 \cos 2\theta_\nu & \delta m^2 \sin 2\theta_\nu \\ \delta m^2 \sin 2\theta_\nu & \delta m^2 \cos 2\theta_\nu \end{pmatrix} \begin{pmatrix} a_e \\ a_\mu \end{pmatrix}$$

Note that the common phase has been ignored: it can be absorbed into the overall phase of the coefficients a_e and a_μ , and thus has no consequence. The matrix above is called the *mass matrix in the flavor basis*. If one were to diagonalize the mass matrix, the eigenvectors would be the mass eigenstates and the difference between the eigenvalues would be $m_2 - m_1$.

4.3 The Mikheyev-Smirnov-Wolfenstein mechanism

The view of neutrino oscillations changed radically when Mikheyev and Smirnov showed in 1985 that the density dependence of the neutrino effective mass, a phenomenon first discussed by Wolfenstein in 1978, could greatly enhance oscillation probabilities: a ν_e is adiabatically transformed into a ν_μ as it traverses a critical density within the sun. It became clear that the sun was not only an excellent neutrino source, but also a natural regenerator for cleverly enhancing the effects of flavor mixing.

While the original work of Mikheyev and Smirnov was numerical, their phenomenon was soon understood analytically as a level-crossing problem. If one writes the neutrino wave function in matter in the same way we did at the end of section 4.2

$$|\nu(x)\rangle = a_e(x)|\nu_e\rangle + a_\mu(x)|\nu_\mu\rangle$$

where x is the coordinate along the neutrino's path, the evolution of $a_e(x)$ and $a_\mu(x)$ is governed by

$$i\frac{d}{dx} \begin{pmatrix} a_e \\ a_\mu \end{pmatrix} = \frac{1}{4E} \begin{pmatrix} 2E\sqrt{2}G_F\rho(x) - \delta m^2 \cos 2\theta_\nu & \delta m^2 \sin 2\theta_\nu \\ \delta m^2 \sin 2\theta_\nu & -2E\sqrt{2}G_F\rho(x) + \delta m^2 \cos 2\theta_\nu \end{pmatrix} \begin{pmatrix} a_e \\ a_\mu \end{pmatrix}$$

where G_F is the weak coupling constant and $\rho(x)$ the solar electron density. If $\rho(x) = 0$, this is exactly our previous result and can be trivially integrated to give the vacuum oscillation solutions of Sec. 4.2. The new contribution to the diagonal elements, $2E\sqrt{2}G_F\rho(x)$, represents the effective contribution to M_ν^2 that arises from neutrino-electron scattering. The

indices of refraction of electron and muon neutrinos differ because the former scatter by charged and neutral currents, while the latter have only neutral current interactions. The difference in the forward scattering amplitudes determines the density-dependent splitting of the diagonal elements of the new matter equation.

It is helpful to rewrite this equation in a basis consisting of the light and heavy local mass eigenstates (i.e., the states that diagonalize the right-hand side of the equation),

$$\begin{aligned} |\nu_L(x)\rangle &= \cos\theta(x)|\nu_e\rangle - \sin\theta(x)|\nu_\mu\rangle \\ |\nu_H(x)\rangle &= \sin\theta(x)|\nu_e\rangle + \cos\theta(x)|\nu_\mu\rangle \end{aligned}$$

The local mixing angle is defined by

$$\begin{aligned} \sin 2\theta(x) &= \frac{\sin 2\theta_\nu}{\sqrt{X^2(x) + \sin^2 2\theta_\nu}} \\ \cos 2\theta(x) &= \frac{-X(x)}{\sqrt{X^2(x) + \sin^2 2\theta_\nu}} \end{aligned}$$

where $X(x) = 2\sqrt{2}G_F\rho(x)E/\delta m^2 - \cos 2\theta_\nu$. Thus $\theta(x)$ ranges from θ_ν to $\pi/2$ as the density $\rho(x)$ goes from 0 to ∞ .

If we define

$$|\nu(x)\rangle = a_H(x)|\nu_H(x)\rangle + a_L(x)|\nu_L(x)\rangle,$$

the neutrino propagation can be rewritten in terms of the local mass eigenstates

$$i\frac{d}{dx}\begin{pmatrix} a_H \\ a_L \end{pmatrix} = \begin{pmatrix} \lambda(x) & i\alpha(x) \\ -i\alpha(x) & -\lambda(x) \end{pmatrix} \begin{pmatrix} a_H \\ a_L \end{pmatrix}$$

with the splitting of the local mass eigenstates determined by

$$2\lambda(x) = \frac{\delta m^2}{2E}\sqrt{X^2(x) + \sin^2 2\theta_\nu}$$

and with mixing of these eigenstates governed by the density gradient

$$\alpha(x) = \left(\frac{E}{\delta m^2}\right) \frac{\sqrt{2}G_F\frac{d}{dx}\rho(x)\sin 2\theta_\nu}{X^2(x) + \sin^2 2\theta_\nu}.$$

The results above are quite interesting: the local mass eigenstates diagonalize the matrix if the density is constant. In such a limit, the problem is no more complicated than our original vacuum oscillation case, although our mixing angle is changed because of the matter effects. But if the density is not constant, the mass eigenstates in fact evolve as the density

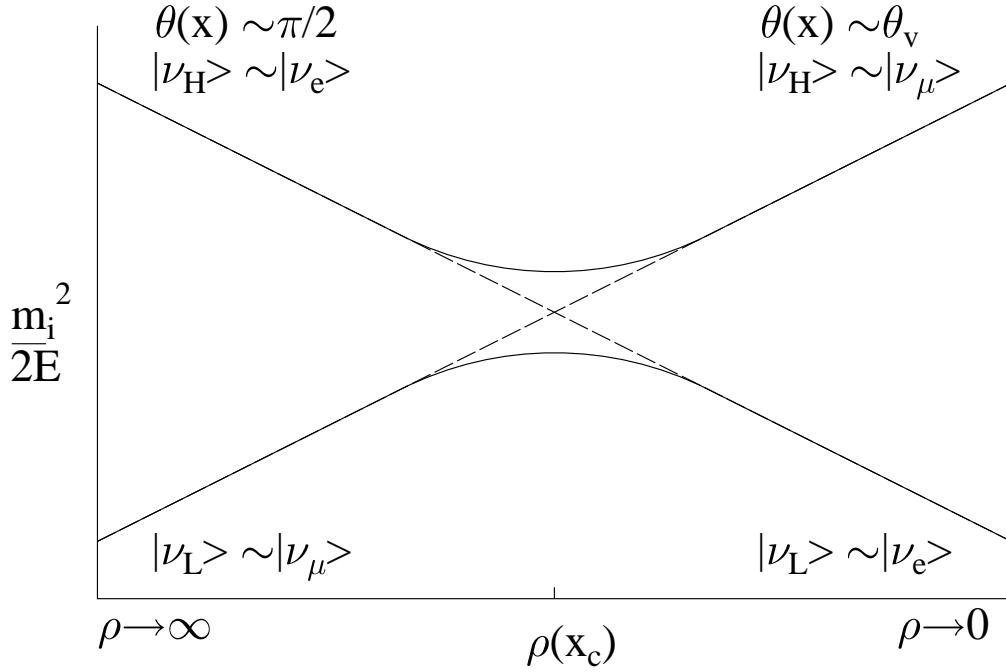


Figure 7: Schematic illustration of the MSW avoided level crossing. The dashed lines correspond to the electron-electron and muon-muon diagonal elements of the M^2 matrix in the flavor basis. Their intersection defines the level-crossing density ρ_c . The solid lines are the trajectories of the light and heavy mass eigenstates. If the electron neutrino is produced at sufficiently high densities and propagates adiabatically, it will follow the heavy-mass trajectory, emerging from the sun as a ν_e .

changes. This is the crux of the MSW effect. Note that the splitting achieves its minimum value, $\frac{\delta m^2}{2E} \sin 2\theta_v$, at a critical density $\rho_c = \rho(x_c)$

$$2\sqrt{2}EG_F\rho_c = \delta m^2 \cos 2\theta_v$$

that defines the point where the diagonal elements of the original flavor matrix cross.

Our local-mass-eigenstate form of the propagation equation can be trivially integrated if the splitting of the diagonal elements is large compared to the off-diagonal elements,

$$\gamma(x) = \left| \frac{\lambda(x)}{\alpha(x)} \right| = \frac{\sin^2 2\theta_v}{\cos 2\theta_v} \frac{\delta m^2}{2E} \frac{1}{\left| \frac{1}{\rho_c} \frac{d\rho(x)}{dx} \right|} \frac{[X(x)^2 + \sin^2 2\theta_v]^{3/2}}{\sin^3 2\theta_v} \gg 1,$$

a condition that becomes particularly stringent near the crossing point,

$$\gamma_c = \gamma(x_c) = \frac{\sin^2 2\theta_v}{\cos 2\theta_v} \frac{\delta m^2}{2E} \frac{1}{\left| \frac{1}{\rho_c} \frac{d\rho(x)}{dx} \Big|_{x=x_c} \right|} \gg 1.$$

The resulting adiabatic electron neutrino survival probability, valid when $\gamma_c \gg 1$, is

$$P_{\nu_e}^{\text{adiab}} = \frac{1}{2} + \frac{1}{2} \cos 2\theta_v \cos 2\theta_i$$

where $\theta_i = \theta(x_i)$ is the local mixing angle at the density where the neutrino was produced.

The physical picture behind this derivation is illustrated in Figure 7. One makes the usual assumption that, in vacuum, the ν_e is almost identical to the light mass eigenstate, $\nu_L(0)$, i.e., $m_1 < m_2$ and $\cos \theta_v \sim 1$. But as the density increases, the matter effects make the ν_e heavier than the ν_μ , with $\nu_e \rightarrow \nu_H(x)$ as $\rho(x)$ becomes large. The special property of the sun is that it produces ν_e s at high density that then propagate to the vacuum where they are measured. The adiabatic approximation tells us that if initially $\nu_e \sim \nu_H(x)$, the neutrino will remain on the heavy mass trajectory provided the density changes slowly. That is, if the solar density gradient is sufficiently gentle, the neutrino will emerge from the sun as the heavy vacuum eigenstate, $\nu_H(0) \sim \nu_\mu$. This guarantees nearly complete conversion of ν_e s into ν_μ s, producing a flux that cannot be detected by the Homestake or SAGE/GALLEX detectors.

But this does not explain the curious pattern of partial flux suppressions coming from the various solar neutrino experiments. The key to this is the behavior when $\gamma_c \lesssim 1$. Our expression for $\gamma(x)$ shows that the critical region for nonadiabatic behavior occurs in a narrow region (for small θ_v) surrounding the crossing point, and that this behavior is controlled by the derivative of the density. This suggests an analytic strategy for handling nonadiabatic crossings: one can replace the true solar density by a simpler (integrable!) two-parameter form that is constrained to reproduce the true density and its derivative at the crossing point

x_c . Two convenient choices are the linear ($\rho(x) = a + bx$) and exponential ($\rho(x) = ae^{-bx}$) profiles. As the density derivative at x_c governs the nonadiabatic behavior, this procedure should provide an accurate description of the hopping probability between the local mass eigenstates when the neutrino traverses the crossing point. The initial and ending points x_i and x_f for the artificial profile are then chosen so that $\rho(x_i)$ is the density where the neutrino was produced in the solar core and $\rho(x_f) = 0$ (the solar surface), as illustrated in the Figure 8. Since the adiabatic result ($P_{\nu_e}^{\text{adiab}}$) depends only on the local mixing angles at these points, this choice builds in that limit. But our original flavor-basis equation can then be integrated exactly for linear and exponential profiles, with the results given in terms of parabolic cylinder and Whittaker functions, respectively. This treatment, called the finite Landau-Zener approximation, has been used extensively in numerical calculations.

We derive a simpler (“infinite”) Landau-Zener approximation by observing that the nonadiabatic region is generally confined to a narrow region around x_c , away from the endpoints x_i and x_f . We can then extend the artificial profile to $x = \pm\infty$, as illustrated by the dashed lines in Figure 8. As the neutrino propagates adiabatically in the unphysical region $x < x_i$, the exact solution in the physical region can be recovered by choosing the initial boundary conditions

$$a_L(-\infty) = -a_\mu(-\infty) = \cos\theta_i e^{-i\int_{-\infty}^{x_i} \lambda(x) dx}$$

$$a_H(-\infty) = a_e(-\infty) = \sin\theta_i e^{i\int_{-\infty}^{x_i} \lambda(x) dx}$$

That is $|\nu(-\infty)\rangle$ will then adiabatically evolve to $|\nu(x_i)\rangle = |\nu_e\rangle$ as x goes from $-\infty$ to x_i . The unphysical region $x > x_f$ can be handled similarly.

With some algebra a simple generalization of the adiabatic result emerges that is valid for all $\delta m^2/E$ and θ_v

$$P_{\nu_e} = \frac{1}{2} + \frac{1}{2} \cos 2\theta_v \cos 2\theta_i (1 - 2P_{\text{hop}})$$

where P_{hop} is the probability of hopping from the heavy mass trajectory to the light trajectory on traversing the crossing point. For the linear approximation to the density,

$$P_{\text{hop}}^{\text{lin}} = e^{-\pi\gamma_c/2}$$

As it must by our construction, P_{ν_e} reduces to $P_{\nu_e}^{\text{adiab}}$ for $\gamma_c \gg 1$. When the crossing becomes nonadiabatic (e.g., $\gamma_c \ll 1$), the hopping probability goes to 1, allowing the neutrino to exit the sun on the light mass trajectory as a ν_e , i.e., no conversion occurs.

Thus there are two conditions for strong conversion of solar neutrinos: there must be a level crossing (that is, the solar core density must be sufficient to render $\nu_e \sim \nu_H(x_i)$ when it is first produced) and the crossing must be adiabatic. The first condition requires that $\delta m^2/E$ not be too large, and the second $\gamma_c \gtrsim 1$. The combination of these two constraints, illustrated in Figure 9, defines a triangle of interesting parameters in the $\frac{\delta m^2}{E} - \sin^2 2\theta_v$ plane, as Mikheyev and Smirnov found by numerical integration. A remarkable feature of this triangle is that

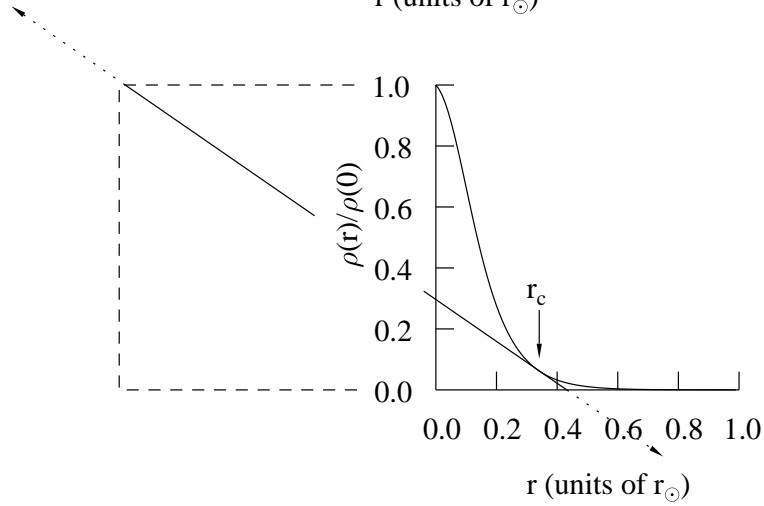
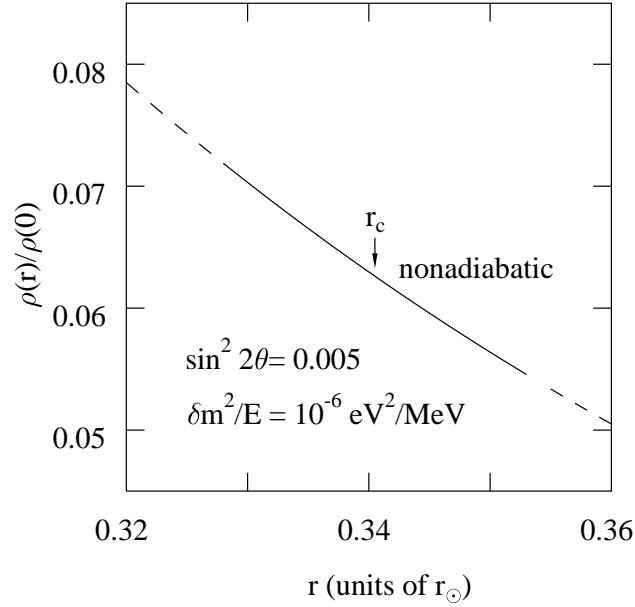


Figure 8: The top figure illustrates, for one choice of $\sin^2 2\theta$ and δm^2 , that the region of nonadiabatic propagation (solid line) is usually confined to a narrow region around the crossing point r_c . In the lower figure, the solid lines represent the solar density and a linear approximation to that density that has the correct initial and final values, as well as the correct density and density derivative at r_c . Thus the linear profile is a very good approximation to the sun in the vicinity of the crossing point, while also building in the correct adiabatic behavior (governed by the starting and ending densities). The MSW equations can be solved analytically for this linear wedge. By extending the wedge to $\pm\infty$ (dotted lines) and assuming adiabatic propagation in these regions of unphysical density, one obtains the simple Landau-Zener result.

strong $\nu_e \rightarrow \nu_\mu$ conversion can occur for very small mixing angles ($\sin^2 2\theta \sim 10^{-3}$), unlike the vacuum case.

One can envision superimposing on Figure 9 the spectrum of solar neutrinos, plotted as a function of $\frac{\delta m^2}{E}$ for some choice of δm^2 . Since Davis sees *some* solar neutrinos, the solutions must correspond to the boundaries of the triangle in the figure. The horizontal boundary indicates the maximum $\frac{\delta m^2}{E}$ for which the sun's central density is sufficient to cause a level crossing. If a spectrum properly straddles this boundary, we obtain a result consistent with the Homestake experiment in which low energy neutrinos (large $1/E$) lie above the level-crossing boundary (and thus remain ν_e 's), but the high-energy neutrinos (small $1/E$) fall within the unshaded region where strong conversion takes place. Thus such a solution would mimic nonstandard solar models in that only the ^8B neutrino flux would be strongly suppressed. The diagonal boundary separates the adiabatic and nonadiabatic regions. If the spectrum straddles this boundary, we obtain a second solution in which low energy neutrinos lie within the conversion region, but the high-energy neutrinos (small $1/E$) lie below the conversion region and are characterized by $\gamma \ll 1$ at the crossing density. (Of course, the boundary is not a sharp one, but is characterized by the Landau-Zener exponential). Such a nonadiabatic solution is quite distinctive since the flux of pp neutrinos, which is strongly constrained in the standard solar model and in any steady-state nonstandard model by the solar luminosity, would now be sharply reduced. Finally, one can imagine "hybrid" solutions where the spectrum straddles both the level-crossing (horizontal) boundary and the adiabaticity (diagonal) boundary for small θ , thereby reducing the ^7Be neutrino flux more than either the pp or ^8B fluxes.

What are the results of a careful search for MSW solutions satisfying the Homestake, Kamiokande/SuperKamiokande, and SAGE/GALLEX constraints? Many authors had answered this question by 1998, obtaining results like those in a figure that will be shown in Section 4.5. The preferred solution (i.e., the best fit) corresponded to a region surrounding $\delta m^2 \sim 6 \cdot 10^{-6} eV^2$ and $\sin^2 2\theta_v \sim 6 \cdot 10^{-3}$: this is the hybrid case described above. It is commonly called the small-angle solution. A second, large-angle solution exists, corresponding to $\delta m^2 \sim 10^{-5} eV^2$ and $\sin^2 2\theta_v \sim 0.6$.

These solutions can be distinguished by their characteristic distortions of the solar neutrino spectrum. The survival probabilities $P_{\nu_e}^{\text{MSW}}(E)$ for the small- and large-angle parameters given above are shown as a function of E in Figure 10.

The MSW mechanism provides a natural explanation for the pattern of observed solar neutrino fluxes. While it requires profound new physics, both massive neutrinos and neutrino mixing are expected in extended models.

A definitive answer to the question of the relevance of the MSW to solar neutrino oscillation came from the Sudbury Neutrino Observatory. But before we discuss this, we turn to

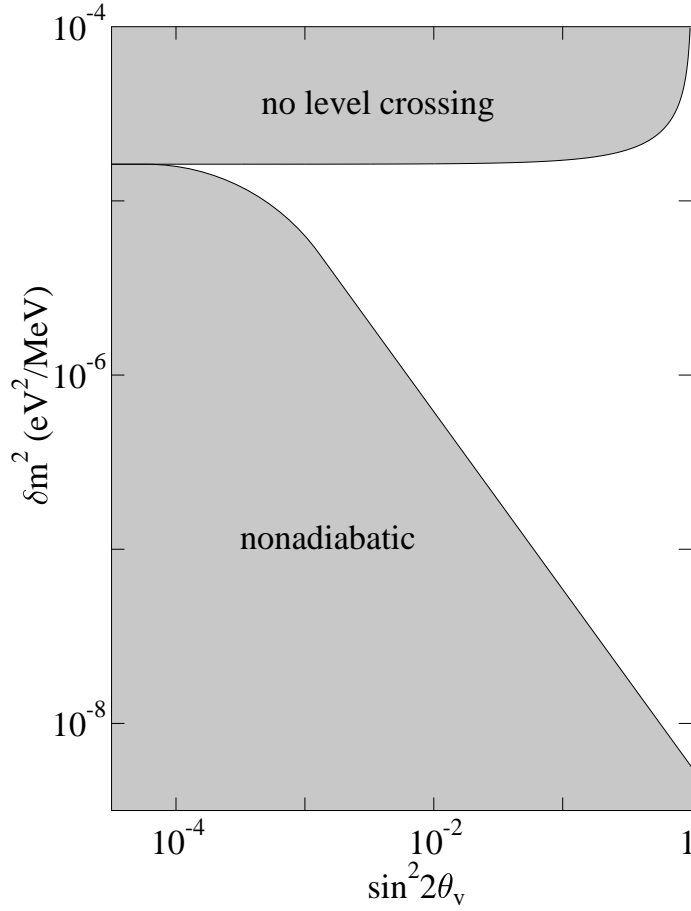


Figure 9: MSW conversion for a neutrino produced at the sun's center. The upper shaded region indicates those $\delta m^2/E$ where the vacuum mass splitting is too great to be overcome by the solar density. Thus no level crossing occurs. The lower shaded region indicates where the level crossing is nonadiabatic (γ_c less than unity). The unshaded region corresponds to adiabatic level crossings where strong $\nu_e \rightarrow \nu_\mu$ will occur.

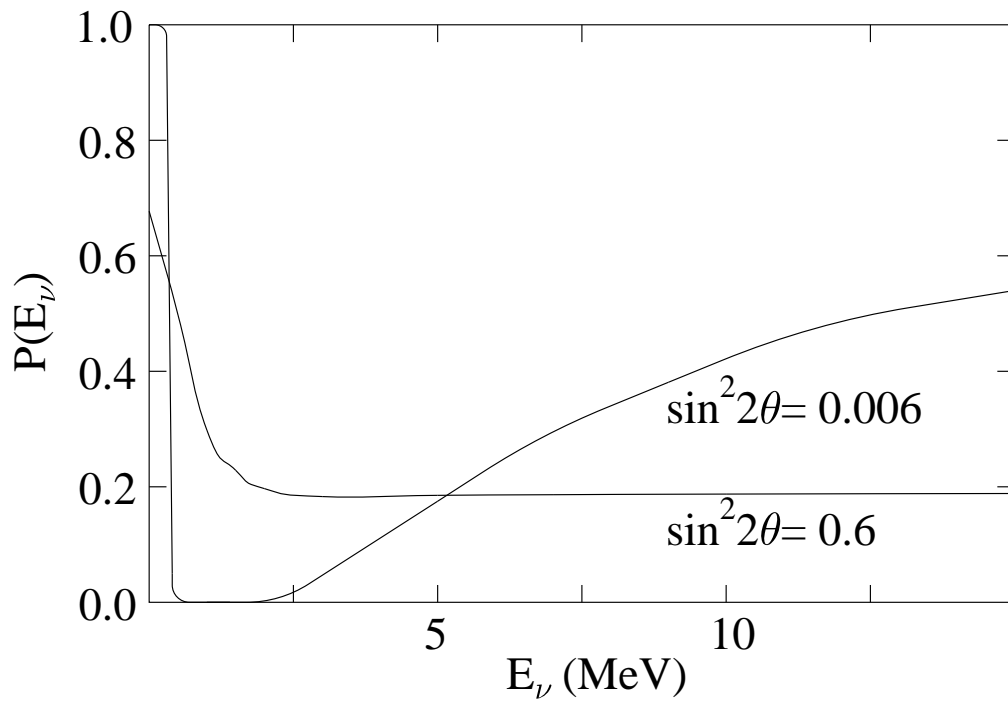


Figure 10: The MSW survival probabilities $P(E_\nu)$ for typical small-angle and large-angle solutions.

another result from 1998 that showed neutrinos oscillate.

4.4 Atmospheric neutrinos: the discovery of neutrino mass

When high energy cosmic rays strike the earth's atmosphere a multitude of secondary particles are produced, most of which travel at nearly the speed of light in the same direction as the incident cosmic ray. Many of the secondaries are pions and kaons, which decay into electrons, muons, and electron and muon neutrinos and antineutrinos. These neutrinos reach and pass through the earth. The fluxes are large: about a hundred such cosmic ray-induced neutrinos pass through each of us every second. Yet because these particles react weakly, only one interaction is expected per human body every thousand years! Thus a considerably larger target is required for a reasonable event rate. In SuperKamiokande, the massive 50,000 ton water detector that replaced the original 3000 ton Kamiokande detector, one event occurs every 90 minutes. The energies of these neutrinos (typically 1 GeV) are sufficiently high to produce either electrons or muons, depending on the neutrino flavor. As these charged particles pass through the water, they produce Cerenkov radiation. However, the Cerenkov ring produced by an energetic electron is more diffuse than the relatively clean ring of a muon. This allows the experimenters to distinguish electrons from muons with about 98% accuracy. Since the charged lepton tends to travel in the same direction as the incident neutrino, the experimenters can thus deduce both the flavor and the direction of neutrinos that react in the water.

A decade ago it was already apparent that atmospheric neutrino rates seen in existing detectors were anomalous. Using known cross sections and decay rates theorists had predicted about twice as many muon neutrinos as electron neutrinos from cosmic ray events. For example, a π^+ decays into an e^+ , a ν_e , a ν_μ , and a $\bar{\nu}_\mu$. That is, two muon neutrinos are produced, but only one ν_e . However, most of the early atmospheric neutrino experiments found the electron-to-muon ratio from neutrino reactions to be approximately unity. The very precise measurements made with SuperKamiokande appear to show that the ratio has this unexpected value because of a deficit in muon-like events—the electron event rate is about as expected. The muon deficit has a strong zenith angle dependence, with the largest suppression associated with atmospheric neutrinos coming from below, *e.g.*, originating on the opposite side of the earth. Such a dependence of the muon-to-electron ratio on distance is a signature of neutrino oscillations, as we have noted. The most plausible interpretation of the SuperKamiokande data is that atmospheric ν_μ 's are oscillating into ν_τ 's, which are not observed because the ν_τ 's are too low in energy to produce τ 's in SuperKamiokande. The strong suppression in the ν_μ flux is characteristic of maximal mixing ($\theta \sim \pi/4$), while the zenith angle dependence indicates that the oscillation length is comparable to the earth's diameter. The corresponding δm^2 is $\sim 2 \cdot 10^{-3} \text{ eV}^2$. Thus this mass difference suggests that at least one neutrino must have a mass $\gtrsim 0.05 \text{ eV}$. The quality of the SuperKamiokande data – the statistical error on the muon-to-electron event rate is well below 10% and there is remarkable consistency between the sub-GeV and multi-GeV data sets and between the fully- and partially-contained data sets – provides a powerful argument that oscillations have been

observed. Because the zenith-angle dependence shows that the ν_μ flux depends on distance, the atmospheric data provide direct proof of oscillations. Thus this may be our strongest evidence for massive neutrinos and for the incompleteness of the standard model.

There is another remarkable aspect of the atmospheric neutrino results. One can view this result in terms of the seesaw mechanism. In the case of the ν_τ we concluded from the atmospheric neutrino data that its mass might be ~ 0.05 eV. A reasonable choice for m_D is the mass of the corresponding third generation quark, the top quark, $m_D \sim 200$ GeV. It follows that $m_R \sim 10^{14}$ GeV! Thus tiny neutrino masses might be our window on physics at enormous energy scales. This large mass m_R is interesting because there is an independent argument, based on observations that the weak, electromagnetic, and strong interactions would all have approximately the same strength at $\sim 10^{16}$ GeV, that suggests a very similar value for the “grand unification scale.” This has led many in the community to hope that the pattern of neutrino masses now being discovered may help us probe the structure of the theory that lies beyond the standard model.

4.5 SNO and the resolution of the solar neutrino problem

The atmospheric neutrino results measure one mass difference, let’s call it m_{23}^2 . The analysis that accounts for the experimental results is based on vacuum oscillations. The mixing angle was maximal – a result few theorists anticipated.

After the Cl, SAGE/GALLEX, and Kamioka/SuperKamioka experiments, an MSW analysis of the results yielded the solar-neutrino solutions shown in Figure 12. There was a small-mixing-angle (SMA) solution, and large-mixing-angle (LMA) solution, and a low-mass-difference and low-probability (LOW) solution. There was also some possibility that a very-low-mass-difference “just-so” vacuum oscillation solution fit the data – one where the oscillation length is tuned to the earth-sun distance. This is not shown in the figure.

Because both charged and neutral currents contribute to the reaction important to SuperKamiokande,

$$\nu_x + e^- \rightarrow \nu_x + e^-$$

the experimentalists cannot easily distinguish ν_{es} from the $\nu_\mu s$ and $\nu_\tau s$: the detector records both fluxes, though with a reduced sensitivity (0.15) for the heavy-flavor types. The reaction produces energetic recoil electrons which generate Cerenkov radiation that is recorded in an array of phototubes surrounding the detector. As the cross section is sharply forward peaked, the correlation with the position of the sun can be used to “cut” background contributions associated with cosmic rays and radioactivity in the rock walls surrounding the detector. Because the threshold for electron detection is ~ 6 MeV, only the high energy portion of the ^8B solar neutrino flux is measured. These are the same neutrinos that dominate the radiochemical measurements of Ray Davis: Superkamiokande confirmed that this flux was substantially below that predicted by the standard solar model (SSM)

$$\phi_{SSM}(\nu_x) = 5.44 \times 10^6 \text{ cm}^{-2}\text{sec}^{-1}$$

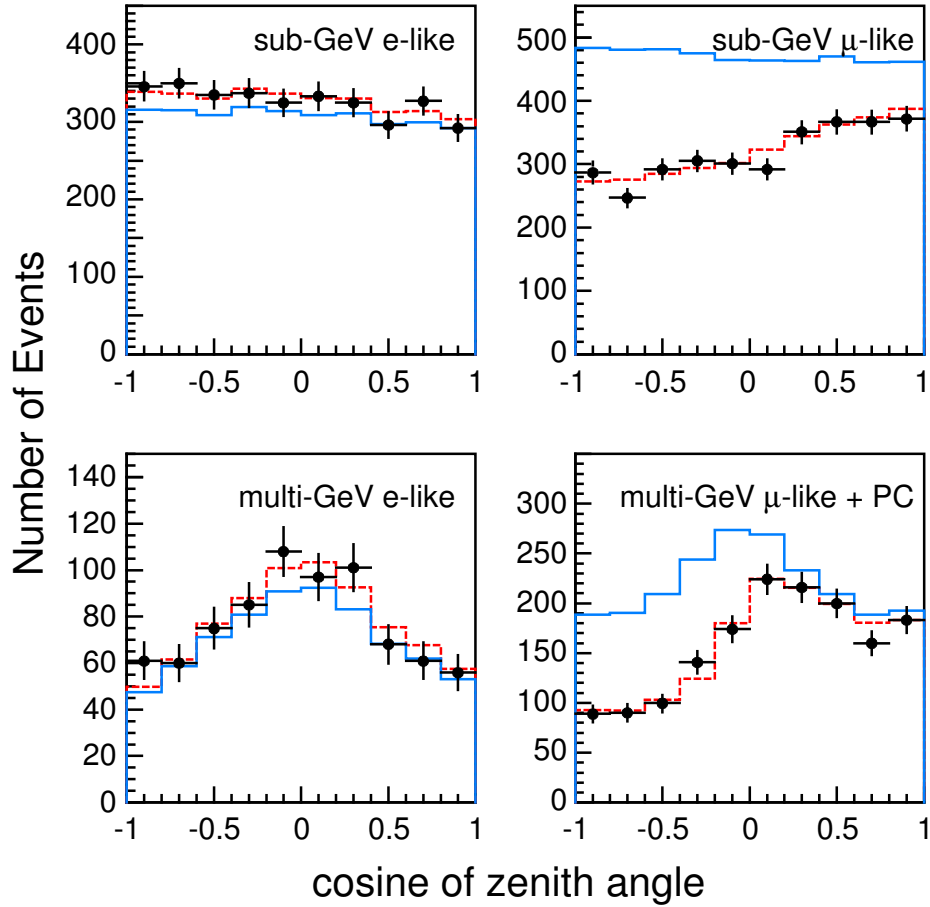


Figure 11: The Super-Kamiokande atmospheric neutrino results showing excellent agreement between the predicted (blue lines) and observed electron-like events, but a sharp depletion in the muon-like events for neutrinos coming from below, through the earth. The results are fit very well by the assumption of $\nu_\mu \rightarrow \nu_\tau$ oscillations with maximal mixing (red lines).

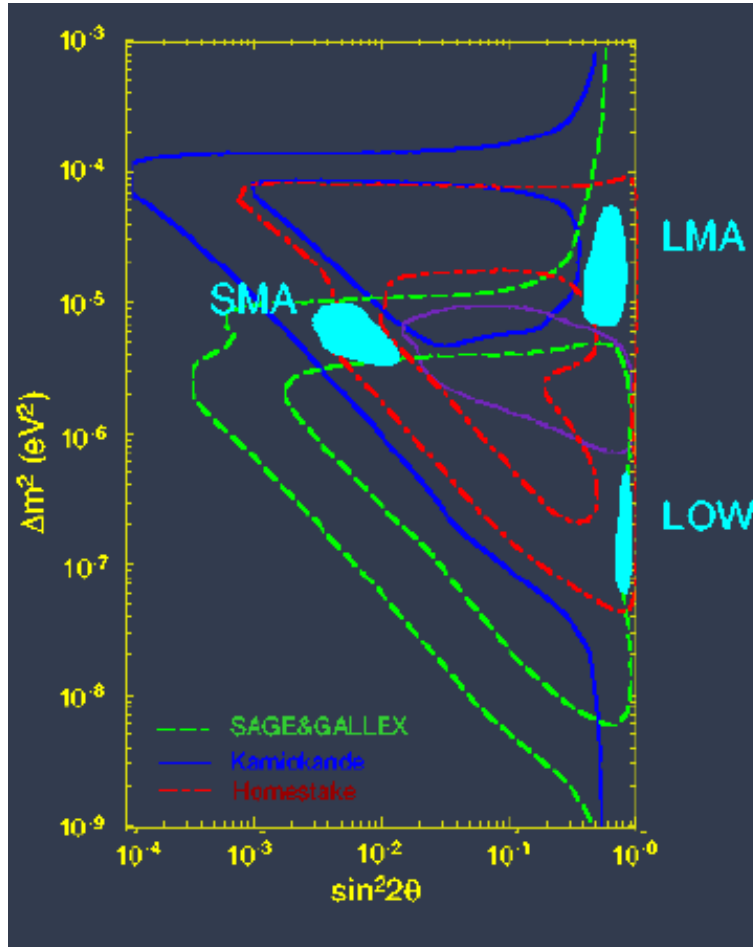
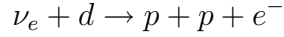
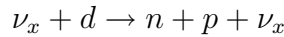


Figure 12: Prior to SNO, this figure illustrates the regions in the $\delta m^2 - \sin^2 2\theta$ plane that were candidates to solve the Cl/Ga/Kamikande/Super-Kamiokande solar neutrino puzzle.

The key idea behind the Sudbury Neutrino Observatory (SNO) was construction of a detector that would have multiple detection channels, recording the ν_e s by one reaction and the total flux of all neutrinos (ν_e s + ν_μ s + ν_τ s) by another. This was accomplished by replacing the ordinary water in a water Cerenkov detector with heavy water – D₂O instead of H₂O. The charged-current (CC) channel that records the ν_e s is analogous to the reaction used in the Davis detector



As the electron produced in this reaction carries off most of the neutrino energy, its detection in the SNO detector (by the Cerenkov light it generates) allows the experimentalists to determine the spectrum of solar ν_e s, not just the flux. A second reaction, the neutral current (NC) breakup of deuterium, gives the total flux, independent of flavor (the ν_e , ν_μ , and ν_τ cross sections are identical),



The only signal for this reaction in a water Cerenkov detector is the neutron, which can be observed as it captures via the (n, γ) reaction. SNO is currently operating with salt added to the water, as Cl in the salt is an excellent (n, γ) target, producing about 8 MeV in γ s.

While the strategy may sound straightforward, producing such a detector was an enormous undertaking. The needed heavy water – worth about \$300M – was available through the Canadian government because of its CANDU reactor program. The single-neutron detection required for the neutral current reaction is possible only if backgrounds are extremely low. For this reason the detector had to be placed very deep underground, beneath approximately two kilometers of rock, so that cosmic-ray muon backgrounds would be reduced to less than 1% of that found in the SuperKamiokande detector. The experimentalists found the needed site in an active nickel mine, the Sudbury mine in Ontario, Canada, where they worked with the miners to carve out a 10-story-high cavity on the mine’s 6800-ft level. Trace quantities of radioactivity were another background concern: if a thimblefull of dust were introduced into the massive cavity during construction, the resulting neutrons from U and Th could cause the experiment to fail. Thus, despite the mining activities that continued around them, the experimentalists constructed their detector to the strictest cleanroom standards. The detector also provided a third detection channel, neutrino elastic scattering (ES) off electrons, which we have noted is sensitive to ν_e s and, with reduced sensitivity, ν_μ s and ν_τ s.

The ES reaction, of course, provides SNO a direct cross check against SuperKamiokande. SNO’s threshold for measuring these electrons is about 5 MeV. Assuming no oscillations, SNO’s detection rate is equivalent to a ν_e flux of

$$\phi_{SNO}^{ES} = 2.39 \pm 0.34(\text{stat}) \pm 0.15(\text{syst}) \times 10^6 \text{ cm}^{-2}\text{sec}^{-1},$$

a result in excellent accord with that from SuperKamiokande,

$$\phi_{SK}^{ES} = 2.32 \pm 0.03(\text{stat}) \pm 0.06(\text{syst}) \times 10^6 \text{ cm}^{-2}\text{sec}^{-1}.$$

The greater accuracy of the SuperKamiokande result reflects the larger mass (50 kilotons) and longer running time of the Japanese experiment. (SNO contains, in addition to the one kiloton of heavy water in its central acrylic vessel, an additional seven kilotons of ordinary water that surrounds the central vessel, helping to shield it.)

The crucial new information provided by SNO comes from the two reactions on deuterium. The CC current channel is only sensitive to ν_e s. Under the assumption of an undistorted ${}^8\text{B}$ neutrino flux, SNO experimentalists deduced

$$\phi_{SNO}^{CC}(\nu_e) = 1.75 \pm 0.07(\text{stat}) \pm 0.12(\text{sys}) \pm 0.05(\text{theory}) \times 10^6 \text{ cm}^{-2}\text{sec}^{-1}.$$

The CC flux is less than that deduced from the ES rate, indicating that ν_μ s and ν_τ s must be contributing to the later. From the difference between the SuperKamiokande ES and the SNO CC results

$$\delta\phi = 0.57 \pm 0.17 \times 10^6 \text{ cm}^{-2}\text{sec}^{-1}$$

and recalling that the ν_μ/ν_τ ES cross section is only 0.15 that for the ν_e , one deduces the heavy-flavor contribution to the solar neutrino flux

$$\phi(\nu_\mu/\nu_\tau) = 3.69 \pm 1.13 \times 10^6 \text{ cm}^{-2}\text{sec}^{-1}.$$

That is, approximately two-thirds of the solar neutrino flux is in these flavors.

While the first SNO analysis was done in the manner described above, a second publication gave the long awaited NC results. This allowed a direct and very accurate determination of the flavor content of solar neutrinos, without the need for combining results from two experiments. The published NC results were obtained without the addition of salt to the detector: the neutron was identified by the 6.25 MeV γ ray it produces by capturing on deuterium. The resulting total flux, independent of flavor, is

$$\phi_{SNO}^{NC}(\nu_x) = 5.09 \pm 0.44(\text{stat}) \pm 0.45(\text{syst}) \times 10^6 \text{ cm}^{-2}\text{sec}^{-1}.$$

Combining with the CC signal yields

$$\phi_{SNO}(\nu_e) = 1.76 \pm 0.05(\text{stat}) \pm 0.09(\text{syst}) \times 10^6 \text{ cm}^{-2}\text{sec}^{-1}$$

$$\phi_{SNO}(\nu_\mu/\nu_\tau) = 3.41 \pm 0.45(\text{stat}) \pm 0.46(\text{syst}) \times 10^6 \text{ cm}^{-2}\text{sec}^{-1}$$

The presence of heavy-flavor solar neutrinos and thus neutrino oscillations is confirmed at the 5.3σ level! Furthermore the total flux is in excellent agreement with the predictions of the SSM— an important vindication of stellar evolution theory.

The SNO analysis is summarized in Figures 13, which shows the three bands corresponding to the CC, NC, and ES measurements coinciding in a single region. These results can now be combined with other solar neutrino measurements to determine the parameters – the mixing

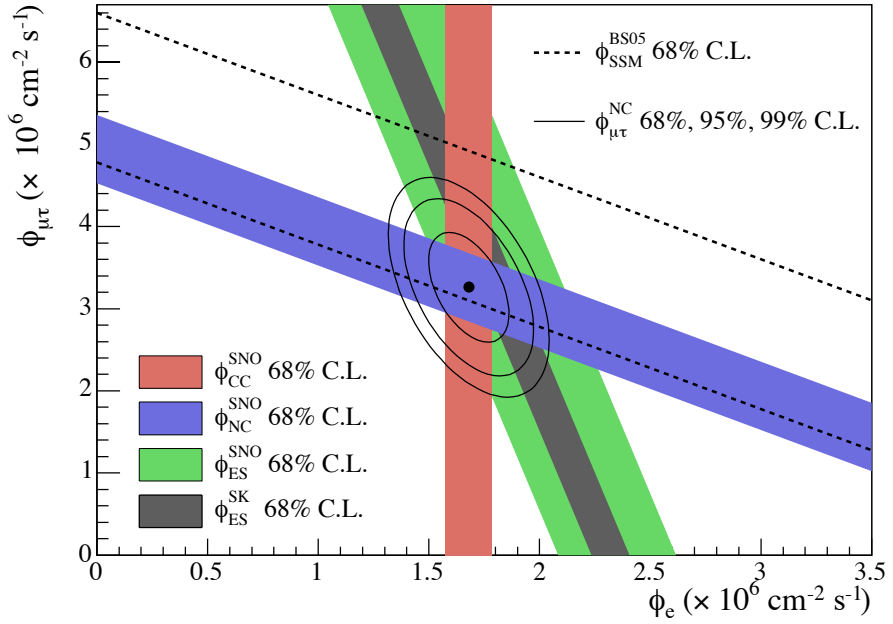
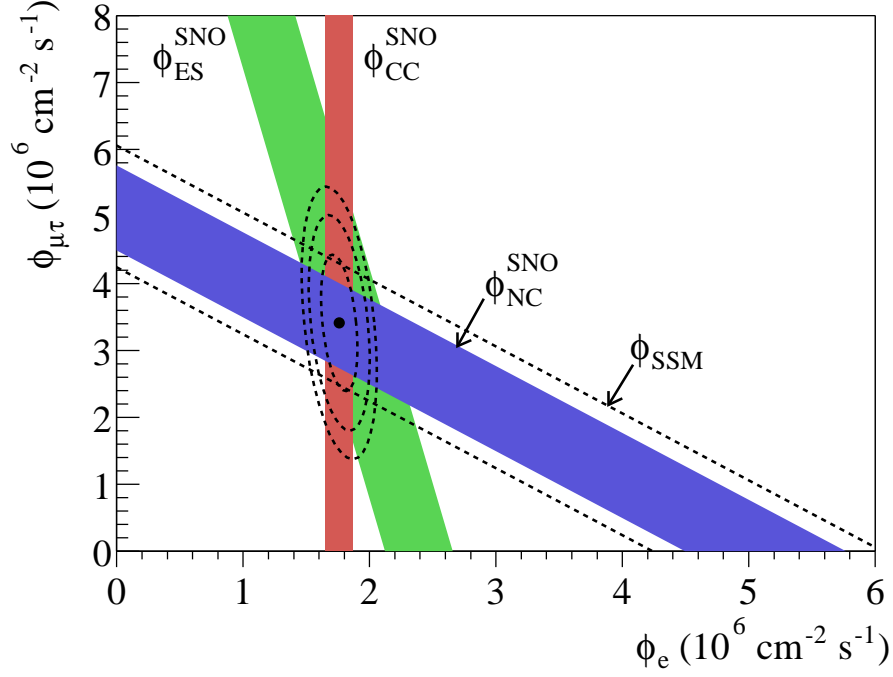


Figure 13: The top and bottom figures correspond to the initial and latest SNO results. The analysis divides the flux of ${}^8\text{B}$ solar neutrinos into ν_μ/ν_τ and ν_e flavors. The diagonal bands show the total ${}^8\text{B}$ flux as predicted by the SSM (dashed lines) and that measured with the NC reaction in SNO (solid band). The widths of these bands represents $\pm 1\sigma$ errors. The bands intersect in a single region for $\phi(\nu_e)$ and $\phi(\nu_\mu/\nu_\tau)$, indicating that the combined flux results are consistent with neutrino flavor transformation assuming no distortion in the ${}^8\text{B}$ neutrino energy spectrum.

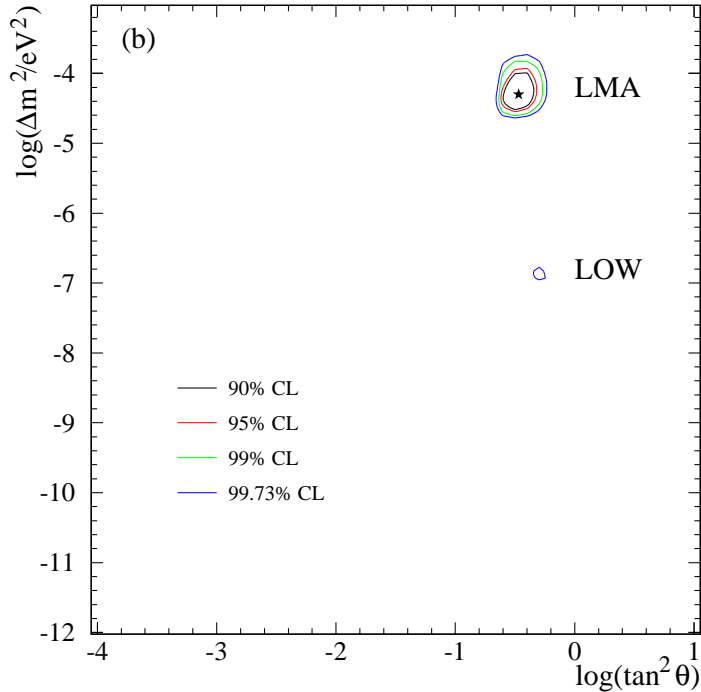


Figure 14: For two-flavor mixing, the values of the mass difference and mixing angle consistent with the data on solar neutrinos, following the initial SNO results. At 99% confidence level the addition of SNO data isolates a unique, large-mixing-angle solution.

angle and mass-squared difference – governing the oscillations. Before SNO produced results, there were several contending solutions, though the data favored one characterized by a small mixing angle (thus called the SMA solution). Figure 14 shows that the SNO result has determined an oscillation solution that, at 99% confidence level, is unique – and as in the atmospheric neutrino case, it has a large mixing angle, $\theta_{12} \sim 30$ degrees. This LMA oscillation is clearly distinct from that seen with atmospheric neutrinos, with $\delta m_{12}^2 = m_2^2 - m_1^2$ centered on a region $\sim 8 \times 10^{-5} \text{ eV}^2$.

The discovery that the atmospheric and solar neutrino problems are both due to neutrino oscillations has provided the first evidence for physics beyond the standard model. That neutrinos provided this evidence is perhaps not unexpected: if the standard model is viewed as an effective theory, one largely valid in our low-energy world but missing physics relevant to very high energies, beyond the reach of current accelerators, then a neutrino mass term is the lowest-order correction that can be added to that theory. But a surprise is the large mixing angles characterizing the neutrino oscillations – which contradicts the simple preju-

dice that neutrino mixing angles might be similar to the small angles familiar from quark mixing. Perhaps this simply reinforces something that should have been apparent at the outset: with their small masses and distinctive mixings, neutrinos likely have an underlying mechanism for mass generation that differs from that of the other standard model fermions.

4.6 Terrestrial verification: KamLAND

One remarkable aspect of the solar and atmospheric neutrino discoveries is that the derived oscillation parameters are within the reach of terrestrial experiments. This did not have to be the case – solar neutrinos are sensitive to neutrino mass differences as small as 10^{-12} eV², for which terrestrial experiments would be unthinkable.

The first terrestrial experiment to probe solar neutrino oscillation parameters, KamLAND, very recently reported first results. The acronym KamLAND stands for Kamioka Liquid scintillator Anti-Neutrino Detector. The inner detector consists of one kiloton of liquid scintillator contained in a spherical balloon, 13m in diameter. The balloon is suspended in the old Kamioka cavity (where SuperKamiokande’s predecessor was housed) by Kevlar ropes, with the region between the balloon and an 18m-diameter stainless steel containment vessel filled with additional scintillator (serving to shield the target from external radiation). Several Japanese power reactors are about 180 km from the Kamioka site, and the electron antineutrinos emitted by nuclear reactions in the cores of these reactors can be detected in KamLAND via the inverse beta decay reaction

$$\bar{\nu}_e + p \rightarrow e^+ + n,$$

where the e^+ is seen in coincidence with the delayed 2.2 MeV γ ray produced by the capture of the accompanying neutron on a proton. This coincidence allows the experimentalists to distinguish $\bar{\nu}_e$ reactions from background.

From the reactor operations records, which the power companies have made available, KamLAND experimentalists can calculate the resulting flux at Kamiokande to a precision of $\sim 2\%$, in the absence of oscillations. Thus, if a significant fraction of the reactor $\bar{\nu}_e$ s oscillate into $\bar{\nu}_\mu$ s or $\bar{\nu}_\tau$ s before reaching the detector, a low rate of e^+ /capture- γ -ray coincidences will be evident: this is an example of the “disappearance” oscillation technique we described in I. For the 162 ton/yr exposure so far reported by the KamLAND collaboration, the number of events expected in the absence of oscillations is 86.8 ± 5.6 . But the number measured is 54 – just 61% of the no-oscillation expectation. From the two-neutrino-flavors oscillation survival probability

$$P(\bar{\nu}_e \rightarrow \bar{\nu}_e) \simeq 1 - \sin^2 2\theta_{12} \sin^2 \frac{\delta m_{12}^2 L}{4E_\nu}$$

one obtains the oscillation parameters of the next figure. KamLAND confirms the LMA solution and significantly narrows SNO’s allowed region (the red area in the figure). KamLAND has excellent sensitivity to δm_{12}^2 but less sensitivity to $\sin^2 2\theta_{12}$ (due to uncertainties in the shape of the reactor $\bar{\nu}_e$ spectrum). The result is the separation of the SNO LMA

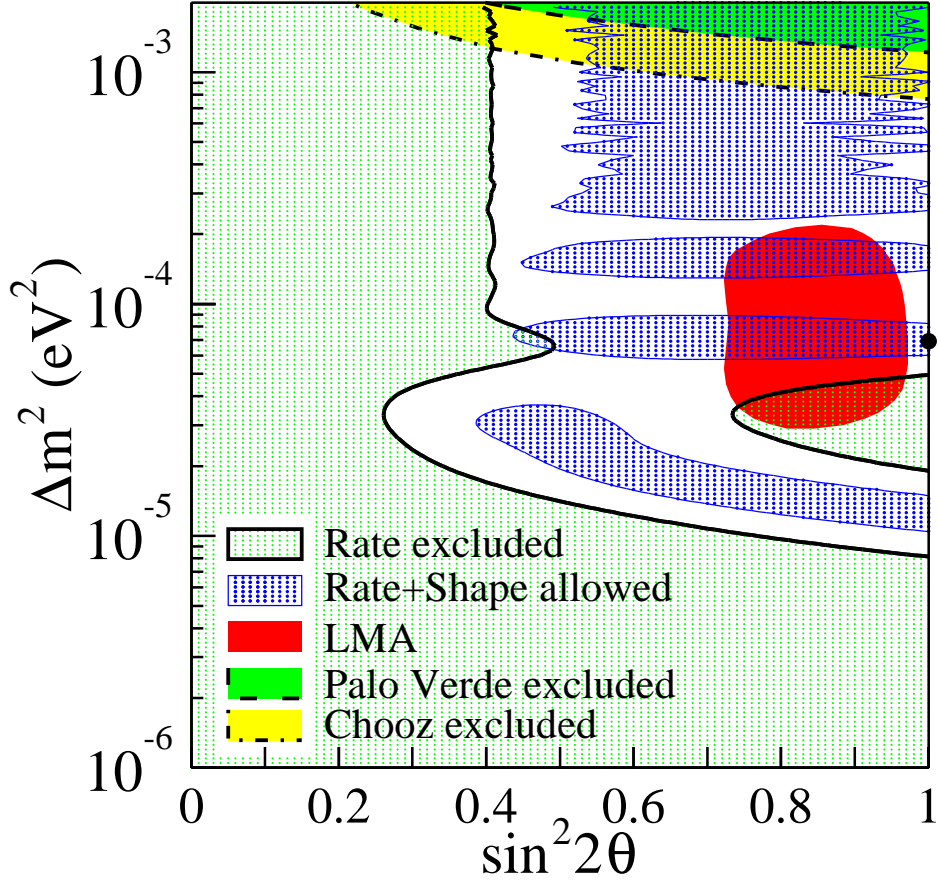


Figure 15: The 95% c.l. LMA allowed region of SNO and other solar neutrino experiments is shown in red. The regions marked “Rate and Shape allowed” show the 95% c.l. KamLAND allowed solutions. The thick dot indicates the best fit to the KamLAND data, corresponding to $\sin^2 2\theta \sim 1.0$ and $\delta m_{12}^2 \sim 6.9 \times 10^{-5} \text{ eV}^2$.

allowed region into two parts, with the best-fit $\delta m_{12}^2 \sim 7 \times 10^{-5} \text{ eV}^2$, but with a larger mass difference $\sim 1.5 \times 10^{-4} \text{ eV}^2$ also fitting well. KamLAND is an excellent example of complementary terrestrial and astrophysical measurements: solar neutrino experiments provide our best constraints on θ_{12} , but KamLAND places the tightest bounds on δm_{12}^2 .

4.7 Summary: what remains to be learned

The net result of all this effort is a determination of δm_{12}^2 , $\theta_{12} \sim 30^\circ$, δm_{23}^2 , $\theta_{23} \sim 45^\circ$

$$\begin{aligned} \begin{pmatrix} \nu_e \\ \nu_\mu \\ \nu_\tau \end{pmatrix} &= \begin{pmatrix} c_{12}c_{13} & s_{12}c_{13} & s_{13}e^{-i\delta} \\ -s_{12}c_{23} - c_{12}s_{23}s_{13}e^{i\delta} & c_{12}c_{23} - s_{12}s_{23}s_{13}e^{i\delta} & s_{23}c_{13} \\ s_{12}s_{23} - c_{12}c_{23}s_{13}e^{i\delta} & -c_{12}s_{23} - s_{12}c_{23}s_{13}e^{i\delta} & c_{23}c_{13} \end{pmatrix} \begin{pmatrix} \nu_1 \\ \nu_2 \\ \nu_3 \end{pmatrix} \\ &= \begin{pmatrix} 1 & & \\ & c_{23} & s_{23} \\ & -s_{23} & c_{23} \end{pmatrix} \begin{pmatrix} c_{13} & & s_{13}e^{-i\delta} \\ & 1 & \\ -s_{13}e^{i\delta} & & c_{13} \end{pmatrix} \begin{pmatrix} c_{12} & s_{12} & \\ -s_{12} & c_{12} & \\ & & 1 \end{pmatrix} \begin{pmatrix} \nu_1 \\ \nu_2 \\ \nu_3 \end{pmatrix} \end{aligned}$$

Here the general transformation between mass and flavor eigenstates is decomposed into its three independent two-by-two rotations. Note that all we know about $\sin\theta_{13}$ comes from reactor $\bar{\nu}_e$ disappearance limits, yielding ≤ 0.17 .

But a lot remains unclear:

- We have mass differences, but no absolute measurement of the masses. Thus we can add amounts to all three masses in such a way as to preserve the mass differences. From laboratory measurements, as we discussed earlier this quarter, the tightest constraint comes from tritium beta decay. This demands that the mass scale is no more than 2.2 eV. A tighter constraint comes from WMAP: the sum of the three masses is no more than 1 eV.
- We don't know the sign of m_{23}^2 . This means that the pair of neutrinos that participates in solar neutrino oscillations can either be the two lightest neutrinos or the two heaviest.
- We don't know θ_{13} . This is a crucial mixing angle for astrophysics (important in a supernova) and also for terrestrial experiments to measure CP violation in long baseline experiments (which look for a difference in $\nu_\mu \rightarrow \nu_e$ vs $\bar{\nu}_\mu \rightarrow \bar{\nu}_e$, other than those induced by matter effects).
- We don't know the value of CP-violating phases. One of these, δ , is involved with θ_{13} in the long-baseline tests for CP violation. Two others are only seen in rather exotic ways, such as in double beta decay.

Thus there is a lot remaining to me done!